Synchrotron Ultrasmall-Angle X-ray Scattering Studies on Tensile Deformation of Poly(1-butene)

Yongfeng Men* and Jens Rieger

BASF Aktiengesellschaft, Polymer Physics, 67056 Ludwigshafen, Germany

Jens Homeyer

Hamburger Synchrotronstrahlungslabor HASYLAB, Deutsches Elektronen-Synchrotron DESY, 22603 Hamburg, Germany

Received August 23, 2004; Revised Manuscript Received October 8, 2004

ABSTRACT: Real-time synchrotron ultrasmall-angle X-ray scattering measurements were performed during the tensile deformation of crystalline phase I poly(1-butene) (P1B). For comparison, high-density polyethylene (HDPE) was also studied. During tensile deformation, the main contribution to the scattering intensity is due to platelike cavities in the case of P1B, whereas very rarely such cavity scattering is observed in the case of HDPE. At small deformations, the platelike cavities were found to occur only in those lamellae whose normals are perpendicular to the stretching direction. This effect is due to the blocky substructure of the crystalline lamellae. At large orientations these cavities reorient turning their normal gradually perpendicular to the stretching direction; this effect is due to the preferential orientation of the polymer chains. Nevertheless, a fraction of the cavities with their normal parallel to the stretching direction are preserved at large deformation. It was found that there exists a critical thickness of cavities below which no stable cavity could be observed. The strain of the cavities with their normal parallel to the stretching direction is proportional to the macroscopic strain but with smaller values.

Introduction

Isotactic poly(1-butene) (P1B) possesses superior creep resistance compared to that of other polyolefins like polyethylene and polypropylene and finds many applications in, e.g., pressurized tanks, tubes, and hot water pipes.[1] P1B always forms the metastable tetragonal phase II crystalline modification when crystallized from the melt state under normal conditions.[2,3] Subject to time, the metastable phase II transforms spontaneously to the stable hexagonal phase I when stored at room temperature.[4] Since P1B is mostly used for long-term applications, the mechanical properties of the stable phase I are technically important. Knowing and understanding morphological changes on a microscopic level during tensile deformation are essential to understanding the macroscopic performance of the material and thus to possible improvement.

Studies of tensile deformation of P1B (phase I) were performed utilizing mostly small- and wide-angle X-ray scattering (SAXS, WAXS),[5−9] transmission electron microscopy (TEM),[5] optical microscopy, and light scattering.[7,10−12] The latter methods are disadvantageous since optical studies require thin films that differ from the bulk samples in terms of stretching behavior, and the TEM method is generally used for ultrathin slice examinations.[5] SAXS and WAXS measurements can be carried out in-situ during the deformation on samples with morphologies similar to bulk material; thus, information like the orientation of crystalline domains and crystalline lamellae can be obtained as a function of strain. However, many microscopic events accompanying tensile deformation of semicrystalline polymers possess characteristic length scales of several hundreds of nanometers or even some micrometers. A typical example is the strain-whitening phenomenon indicating formation of heterogeneities (commonly cavities) at least at a length scale of the wavelength of visible light, i.e., some hundreds of nanometers. It is obvious that this length scale is not accessible for conventional small-angle X-ray scattering measurements. Synchrotron radiation provides the possibility of ultrasmall-angle X-ray scattering (USAXS) and enables the study of the large-scale structure evaluation during the deformation of polymeric materials. The purpose of the present work is thus to study the mechanism of strain-whitening in P1B with stable phase I crystalline modification using online USAXS measurements. As will be reported in the following sections, cavities showing characteristic features occur in P1B extensively.

* Corresponding author. E-mail: yongfeng.men@basf-ag.de.

Experimental Section

Materials. Two P1B samples with different molecular weight were purchased from Aldrich Chemical Co. For comparison, a high-density polyethylene (HDPE) was used which was supplied by BASELL Polyolefin GmbH, Frankfurt, Germany. Samples for tensile tests were obtained by compression-molding the pellets between two plates at 180 °C, yielding polymer plates with a thickness of about 2 mm. Crystallization occurs during cooling the plate to room temperature at a speed of 15 K/min. "Dog bone" tensile bars with a width and a parallel length of 10 mm were obtained with the aid of a punch. Information on molar mass and its distribution, melting point, crystallinity, etc., of the samples is given in Table 1. P1B sample was stored at room temperature for 3 months to allow a complete phase transition from the metastable tetragonal phase II to the stable hexagonal phase I. The phase transition was monitored by wide-angle X-ray diffraction (figures not shown).

Ultrasmall-Angle X-ray Scattering. Ultrasmall-angle X-ray scattering (USAXS) measurements were performed at the synchrotron beamline BW4 at HASYLAB, DESY, Hamburg, Germany. The energy of the X-ray radiation was 8.979 keV, resulting in a wavelength of 0.138 08 nm. The USAXS

10.1021/ma048274k CCC: $27.50
Published on Web 11/16/2004

Table 1. Characterization of Samples

	$M_w \times 10^{-5}$	M_w/M_n	T_m,[a] °C	ϕ_c[a]	d_{ac},[b] nm	d_c,[c] nm
HDPE	3.9	22	133.6	0.64	26.1	16.7
PB18	1.85		120.2	0.49	27.3	13.4
PB57	5.7		126.2	0.58	35.5	20.6

[a] Melting peak position (T_m) and crystallinity (ϕ_c) are derived from differential scanning calorimetry (DSC) heating runs. Heating rate: 15 K/min for HDPE and 20 K/min for P1B. For the calculation of crystallinity a value for the heat of fusion at 100% crystallinity of $\Delta H_{id} = 293$ J/g (for PE) and 125 J/g (for P1B) were used.[32] [b] Long period (d_{ac}) was deduced from small-angle X-ray scattering measurements (see Figure 4). [c] Lamellar thickness values were calculated from the crystallinity and long period value $d_c = d_{ac}\phi_c$.

patterns were recorded by a two-dimensional multiwire proportional Gabriel counter with 512 × 512 pixels, resulting in a detector resolution of 0.4 × 0.4 mm^2. The online stretching experiments were performed with a tensile machine mounted at the beamline.[13] The beam position and the appearance of the sample during the experiment were monitored with a video system. The sample was stretched to the preset elongation at a speed of 5 mm/min, and the USAXS pattern was taken within 2 min before further stretching. The Hencky measure of strain ϵ_H is used as a basic quantity of the extension. ϵ_H is defined as

$$\epsilon_H = \ln(l/l_0) \tag{1}$$

where l_0 and l are the lengths of undeformed and deformed samples. For P1B samples, ϵ_H is obtained by monitoring the separation of equal distanced ink marks on the sample surface. For the sample of HDPE, the changes in sample width are used to derive ϵ_H. Because of the high scattering intensity after deformation and to avoid detector overflow, the vertical beam dimension had to be reduced from 0.27 to 0.1 and 0.075 mm at a true strain (ϵ_H) of 0.15 and 0.50 in the case of the PB18 sample and from 0.17 to 0.1, 0.06, and 0.055 mm at a strain of 0.23, 0.46, and 1.06, respectively, for the PB57 sample. The horizontal beam dimension is fixed at 0.5 mm. In the case of the HDPE sample the beam size is fixed at 0.2 × 0.5 mm^2. The sample-to-detector distance is 12 706 mm. The effective scattering vector q ($q = (4\pi \sin\theta)/\lambda$, where 2θ is the scattering angle and λ the wavelength) range at this distance is 0.025−0.3 nm^{-1}. (q values down to 0.03 nm^{-1} can be reached with well-adjusted Kratky chambers,[14] but with the disadvantage that no two-dimensional scattering data are obtained.) USAXS patterns were background corrected and normalized using the standard procedure at HASYLAB.

The scattering patterns for undeformed samples were first averaged over all directions at constant q, resulting in one-dimensional scattering intensity curves (I vs q). Lorentz correction (multiplication of I with q^2) is performed in order to calculate the long period of the lamellar stacks. For the anisotropic scattering patterns after stretching, rectangular slice cuts (with a width of 10 pixels) passing through the beam center were taken to obtain the scattering intensity profiles parallel (I vs q_v) and perpendicular (I vs q_h) to the stretching direction.

Results and Discussion

Figures 1, 2, and 3 show series of USAXS patterns of PB18, PB57, and HDPE at different strains and in the relaxed state after deformation. In Figure 3, there is a large strain (ϵ_H) gap from 0.35 to 1.26 where scattering patterns are not shown. This is because of the formation of a neck in the HDPE sample. The scattering patterns of HDPE are given only for the sake of comparison, and no deep analysis of the HDPE data will be done here. The undeformed samples give rise to a "scattering circle" with a homogeneous intensity distribution along the circle, as is expected from randomly oriented the stacks of crystalline lamellae embedded in an amorphous matrix. The long period of the lamellar stacks (i.e., the average distance between the midplanes of two adjacent lamellae measured along the lamella normal) of the undeformed samples was calculated using the plots of Lorentz corrected scattering intensities as a function of scattering vector in Figure 4 according to the following equation:

$$d_{ac} = \frac{2\pi}{q_{max}} \tag{2}$$

where d_{ac} is the long period and q_{max} the peak position. The results have been included in Table 1. Since PB57 has a higher crystallinity (derived from DSC measurements) and long period than PB18, it is evident that PB57 has thicker crystalline lamellae than PB18.

Before having a closer look on the differences between the USAXS patterns of P1B and HDPE, attention is drawn to a notable feature being the scattering intensity variation *after* stretching. For both P1B samples, the scattering power increased dramatically whereas it stays relatively constant for HDPE sample. In general, the scattering power is linked to the amount of the heterogeneities (dispersed phase) and the density difference between the heterogeneities and the matrix. The scattering power can be obtained by the following relation:[15]

$$Q = V_{irr}\phi_{hetero}(1 - \phi_{hetero})(\rho^e_{bulk} - \rho^e_{hetero})^2 \propto \int_0^\infty \int_0^\infty I(q_x,q_y)\, dq_x\, dq_y \tag{3}$$

where V_{irr} is the volume of the sample irradiated by X-rays, ϕ_{hetero} is the volume fraction of the heterogeneities, ρ^e_{bulk} and ρ^e_{hetero} are the corresponding electron densities of the matrix and the heterogeneities, and q_x and q_y are the scattering vectors perpendicular and along the stretching direction. In the case of semicrystalline polymers ρ^e_{bulk} and ρ^e_{hetero} correspond to the electron density of the crystalline and amorphous phases. It must be mentioned that the integration in eq 3 cannot be precisely performed in the present work because of the limited range of scattering angles accessed in the experiments. Nevertheless, it is evident that the scattering intensity at large angles is negligible and that the scattering signals hidden by the small beam stop only contribute to a small extent to the total intensity. Qualitatively, the integrated scattering intensity as a measure of the scattering power at different deformations for all three samples is shown in Figure 5. If a stretching run results only in a reorientation or reorganization of the crystallites in the system, no changes in the scattering power is expected. The case of HDPE points to this situation since only a slight increase in the scattering power is observed during deformation. However, a pronounced increase in the scattering power occurs for the two P1B samples, indicating the appearance of structures, e.g., cavities with an electron density differing from that of the constituents of the polymeric phase. Cavities are voids of solid material, thus giving rise to a maximum electron density difference contributing to the scattering power to the power of square ($\rho^e_{bulk}{}^2$ term). For both P1B samples the integrated scattering increases with the strain and reaches a maximum value at a strain of about 0.5 followed by a decrease with further straining.

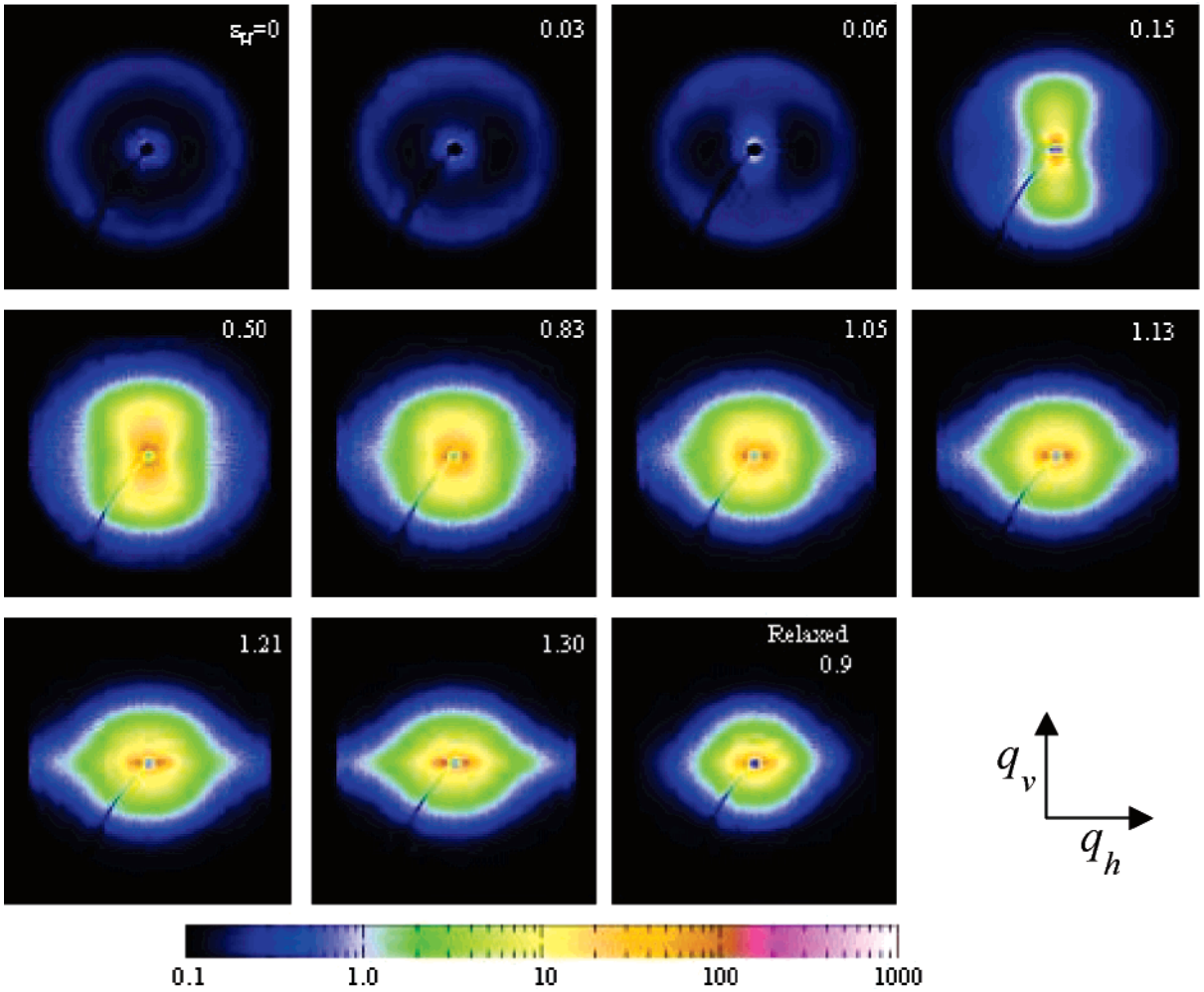

Figure 1. PB18: USAXS patterns taken at different deformations as indicated on the graph. Stretching direction vertical. Arrows indicate the directions of integrating intensity.

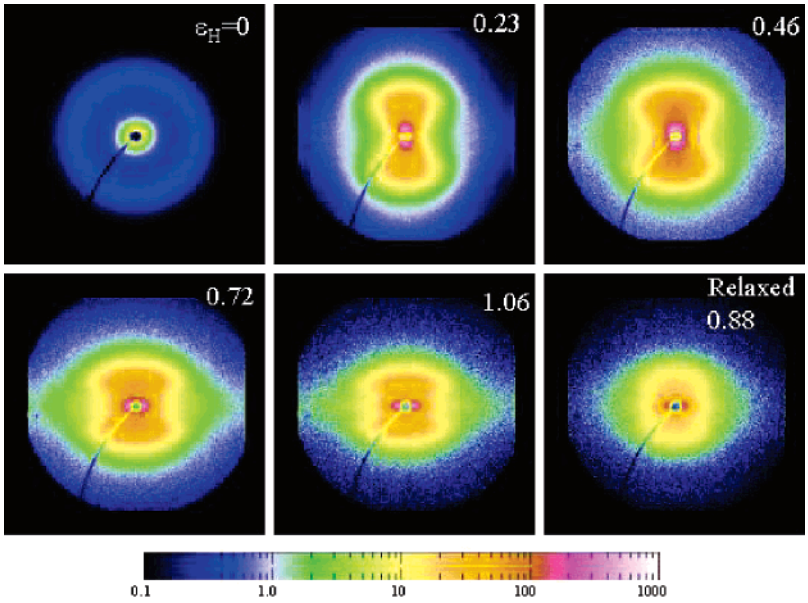

Figure 2. PB57: USAXS patterns taken at different deformations as indicated on the graph. Stretching direction vertical.

The scattering power for HDPE does not vary when the stress is removed whereas it decreases in the case of the P1B samples. Comparing the two P1B samples, one finds a correlation between crystallinity and volume fraction of cavities, indicating that the occurrence of cavities is linked to the presence of crystalline lamellae. Molecular weight is believed to influence the volume fraction of cavities in an indirect way, namely, by affecting the crystallinity of the system. This correlation originates from the fact that cavities do form at small

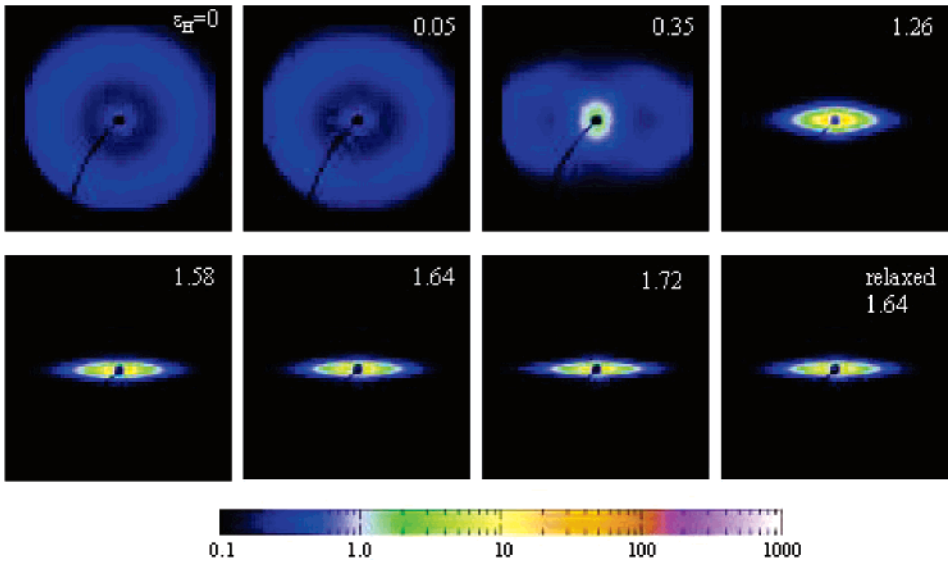

Figure 3. HDPE: USAXS patterns taken at different deformations as indicated on the graph. Stretching direction vertical.

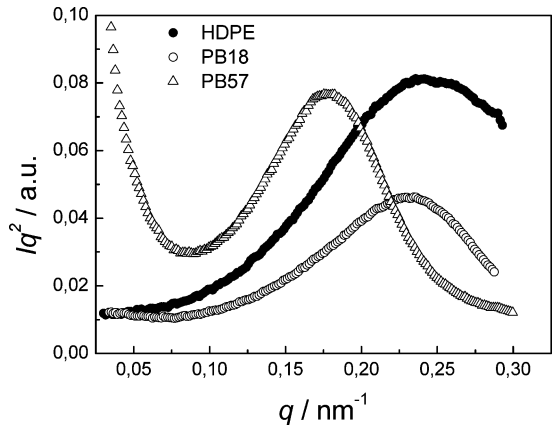

Figure 4. Lorentz corrected intensity Iq^2 as a function of q for undeformed HDPE, PB18, and PB57 samples for calculating the long periods (d_{ac}).

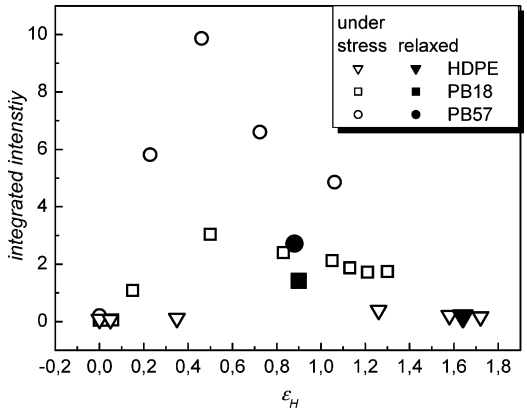

Figure 5. Integrated scattering intensity as a measure of the scattering power of the system at different deformations.

deformations where the crystalline skeleton dominates the mechanical properties of the system.[16−18]

Apart from the crystallinity differences and thus the scattering intensity differences, the USAXS patterns during straining show similar characteristics for the two P1B samples. They, however, differ qualitatively from the USAXS patterns of HDPE. It is well-known that tensile stretching transforms the original spherulite morphology of HDPE into fibrillar assemblies with molecular chains along the stretching direction.[19−21] The equatorial scattering streak in Figure 3 at large deformations ($\epsilon_H > 1.0$) is attributed to the corresponding fibril scattering. Taken a closer look at Figures 1 and 2, it is seen that at small deformation the scattering from lamellae is preserved and that additional intensity appears in the meridional direction. This meridian scattering increases in its intensity strongly up to moderate deformation ($\epsilon_H \sim 0.5$) before decreasing again. Meanwhile, the equatorial scattering appears at moderate deformation and increases with increasing elongation. The USAXS patterns are indicative for the formation of platelike cavities with the normal at first along and then turning perpendicularly to the stretching direction with increase of the elongation. The equatorial scattering spreads to higher q values at large deformations evidencing a thinning process of the perpendicular plate cavities. A natural question arising from the evaluation of the scattering patterns during deformation is why the cavities appear first with their normal along the stretching direction. To understand this, let us consider the microscopic morphology of the P1B samples. P1B exhibits an unusual secondary transition (crystal phase transition). Crystallization of P1B from the melt first yields phase II crystalline lamellae with the amorphous phase of entangled polymeric chains in between. During the transition from crystalline phase II to I global shrinkage is always observed. Accompanying relaxational processes also leave many defects in the crystalline lamellae.[22] This becomes even more evident when the blocky substructure of the lamellae after crystallization is taken into account.[23,24] Blocks exhibit disordered grain boundaries, which could not be included into the transformed phase I crystallites. The shrinkage of the crystalline blocks (densification) results in even more disordered boundaries between the adjacent blocks. These loose block boundaries serve as precursors for the cavities during tensile deformation. Because polymer chains in the crystalline lamellae are in most cases orientated along the lamellar normal, the block boundaries must have their normal perpendicular to polymer chains, i.e., to the lamellar normal. It is clear that only those block boundaries with their normal parallel to the stretching direction are able to develop into cavities. The block boundaries with their normal

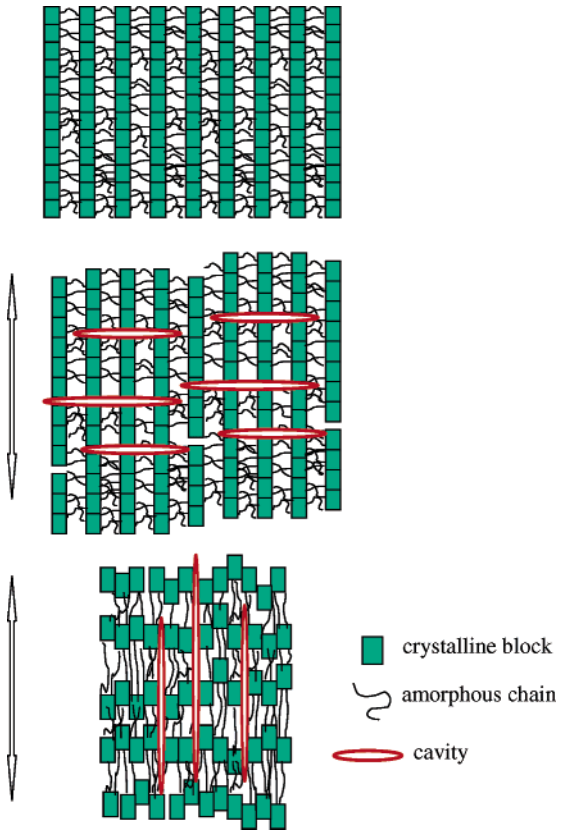

Figure 6. Schematic presentation of cavity formation and transformation upon straining in P1B. The arrows indicate the stress direction. Top: lamellae cluster of undeformed state; middle: at small to moderate deformation; bottom: at late stages of deformation (not to scale).

perpendicular or oriented at some oblique angles to the stretching direction would undergo shear deformation without cavitation. Figure 6 provides a sketch of the situation. To illustrate and emphasize the cavity formation, only those lamellae with their normal perpendicular to the stretching direction are shown in Figure 6. Although the final result is the preferential orientation of the polymer chains along the stretching direction upon deformation, it is the crystalline skeleton that transmits forces at small deformation. This is due to the fact that the morphology of a semicrystalline polymer can be regarded as an interpenetrating network of entangled polymer melt (amorphous phase) and a crystalline skeleton (the crystalline lamellae).[16−18] When the stretching direction is perpendicular to the lamellar normal, the block boundaries open in width and form cavities passing through amorphous phases connecting several lamellae (middle illustration in Figure 6). However, the polymer chains in this case are perpendicular to the stretching direction and thus must turn to the parallel direction at larger deformation. Therefore, a decrease in the scattering intensity along the meridian and an increase along the equator are observed, indicating the transition of the parallel cavities to the perpendicular direction to stretching. This model is in line with earlier findings of Stein et al.:[10,11] on stretching an aged P1B film, the birefringence was found at first to be negative, passing through a maximum negative value and becoming positive at higher elongation. It was concluded that this is because of the preservation of the chain orientation in spherulites during deformation. The preservation of the orientation of the perpendicular lamellae provides the physical basis for the model shown in Figure 6. At the final stage of the deformation, most of the chains must be oriented preferentially along the stretching direction (bottom illustration in Figure 6), and thus the positive birefringence is observed.

To derive quantitative information about the cavities, it must be clarified first that the intensity distribution on the USAXS patterns originates from scattered X-rays and not from the reflected ones. It has been long established that the refraction of X-rays may affect the scattering pattern when the lamellar stacks possess a spacing greater than a critical value (e.g., 96 nm for PE of 70% crystallinity).[25] In the present case, the shape of the cavities is similar to that of crazes that are known to scatter and to reflect X-rays under certain conditions.[26,27] However, a simple method was proposed[27,28] to elucidate whether reflection effects contribute significantly. It consists of tilting the sample a few degrees with respect to the standard orientation where the tensile direction is orthogonal to the incident X-ray. If there were reflected X-rays in the perpendicular case, the intensity must diminish when tilting the sample. We have thus checked in our system by measuring the SAXS patterns of a PB57 sample prestretched to $\epsilon_H = 0.14$ using a laboratory small-angle X-ray scattering system (Nanostar Bruker, Karlsruhe, Germany) at two conditions: stretching direction perpendicular to the incident X-ray (common geometry used for all online measurements) and stretching direction tilted 10° relative to the incident X-ray. The dimension of the sample was fixed with a metal frame to maintain the stress. It turns out that the strong meridional intensity due to the platelike cavities is preserved after tilting. The USAXS intensities are thus due to scattered X-rays.

The meridional and equatorial SAXS scattering intensity profiles are shown in Figures 7 and 8 for the samples of PB18 and PB57, respectively. The equatorial intensity at large deformations shows a smooth decay pointing to a wide distribution of the thicknesses of cavities with their normal perpendicular to the stretching direction. A possible way to evaluate the dimension of these cavities is using the Guinier approximation. When $qR < 1$, the scattering intensity reads $I(q) \sim e^{-q^2R^2/3}$, where R is the radius of gyration of the structure under investigation.[29] Unfortunately, a linear fit of the plots of $\ln[I(q)]$ vs q^2at very small q range yields values of R in the range of 60−70 nm, leading to $qR > 1$, which in turn invalidates the application of the Guinier approximation. Because of this, no attempt was done for calculating the thickness of the cavities with their normal perpendicular to the stretching direction. It is rather only qualitatively discussed here. The meridian scattering intensity shows a characteristic feature, namely, a maximum at a scattering vector that is smaller than the lamellae peak. To check whether this additional peak is due by the specific shape of the cavities, it is useful to consider in a first-order approach the scattering intensity of platelike objects:[15]

$$I(q) = A\,\frac{2\pi}{q^2}(\Delta\rho)^2 d^2\left(\frac{\sin qd/2}{qd/2}\right)^2 \qquad (4)$$

where A is the lateral cross section of the plate, $\Delta\rho$ is the electron density difference between the object and its surrounding phase, and d is the thickness of the plate. It is evident from the above equation that a plot

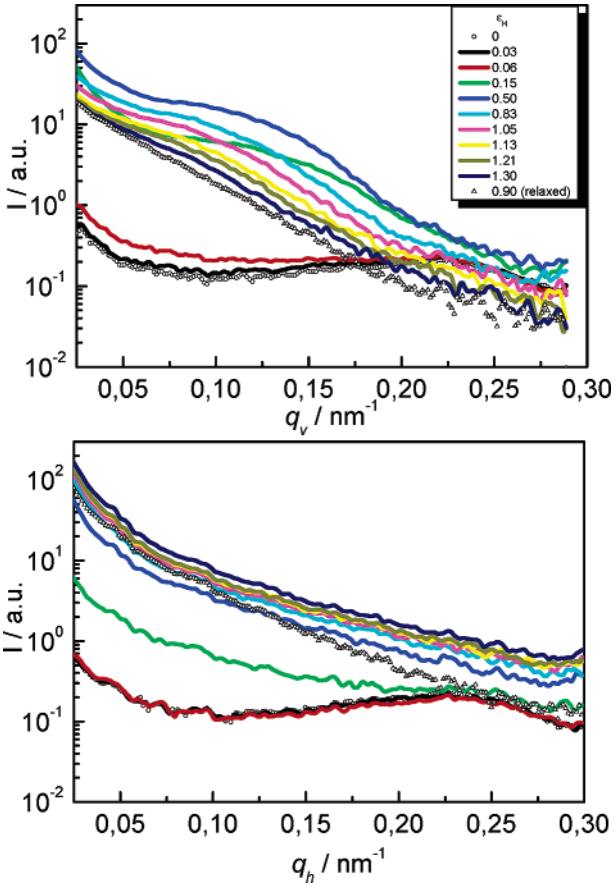

Figure 7. PB18: scattering intensity along vertical (top) and horizontal (bottom) directions at different deformations.

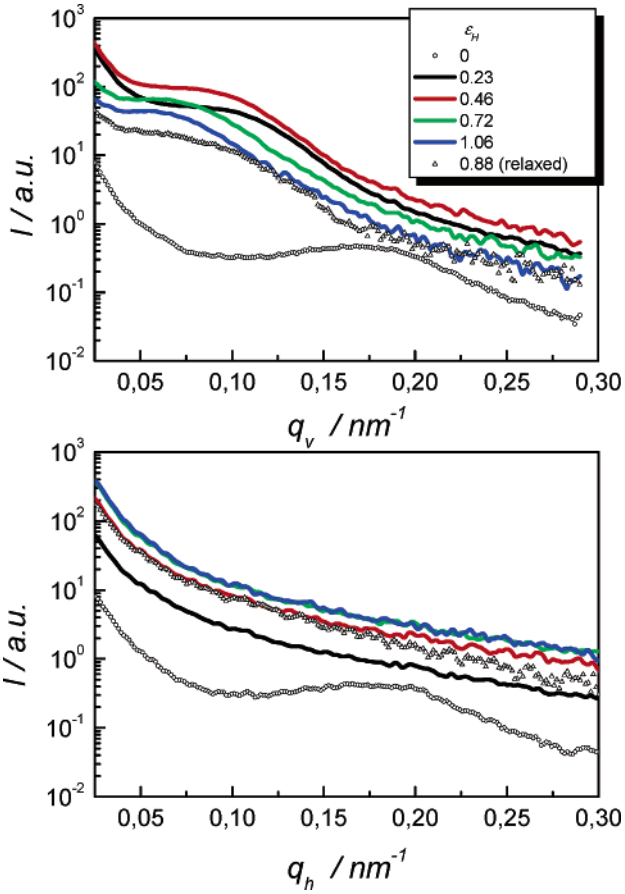

Figure 8. PB57: scattering intensity along vertical (top) and horizontal (bottom) directions at different deformations.

of $I(q)q^2$ vs q yields maxima at $q = 0$ and at $q = [(2n + 1)/d]\pi$ (where $n = 1, 2, 3, ...$). Such plots are presented in Figure 9. In Figure 7, the relaxed PB18 sample shows a rather smooth decay in the intensity and is therefore not included in Figure 9. It is seen that, on one hand, the intensity maximum shifts to smaller q values with the increase of the elongation, indicating a continuous opening of the platelike cavities during stretching. On the other hand, there is a reduction of the cavity number as evidenced by the decrease of the scattering intensity at large deformation. The thickness of the cavities along the stretching direction at different strains can be calculated using the maximum scattering intensity position q_{max} according to

$$d = \frac{3\pi}{q_{max}} \tag{5}$$

The thus obtained d values are given in Figure 10. Two interesting features can be read out directly from Figure 10. First, the cavity thickness over the whole strain range investigated is higher for PB57 than for PB18; second, the cavity thickness for both systems increases linearly with the increase of the elongation. A linear extrapolation of the cavity thickness to the undeformed state ($\epsilon_H = 0$) yields a nonzero value d_0 for both systems. d_0 is thus assumed to be the smallest stable cavity thickness in the system. Using the value of d_0, one is able to calculate the strain of the cavities along its normal by

$$\epsilon_{H,cavities} = \ln\left(\frac{d}{d_0}\right) \tag{6}$$

Figure 11 shows the strain of the cavities as a function of the macroscopic strain. Interestingly, the strain of the cavities for both PB18 and PB57 follows the same trace with the increase of macroscopic strain. However, the cavity strain is much smaller than that of macroscopic strain, indicating that the deformation is locally inhomogeneous in the system despite the macroscopic homogeneous deformation behavior in P1B.

It must be mentioned that cavitation of interlamellar separation type as discussed in the literature[30,31] can be excluded for the following reasons: first, interlamellar separation can only take place with those lamellae having their normal along the stretching direction, which would favor a positive birefringence after deformation which is obviously at variance with the experimental facts;[10,11] second, and most importantly, the dimension of the cavities derived from the meridian scattering intensity distribution is far beyond that of lamellar long spacing after appropriate deformation. If the maximum on the meridian scattering curve after deformation were due to stacks of lamellae, one would obtain a value of 48 nm for a PB18 at small deformation of $\epsilon_H = 0.15$ compared to the long spacing of PB18 at undeformed state of 27.3 nm. If interlamellar separation were to take place, one would expect a gradual increase of the long spacing rather than such an abrupt change.

The thicknesses of the cavities derived from the USAXS data are around 100 nm (compare Figure 10), i.e., much smaller than the wavelength of visible light. This seems contradictory to the strain-whitening phenomenon where much larger heterogeneities would be needed to explain the visible whitening. However, this can be understood when considering the characteristic

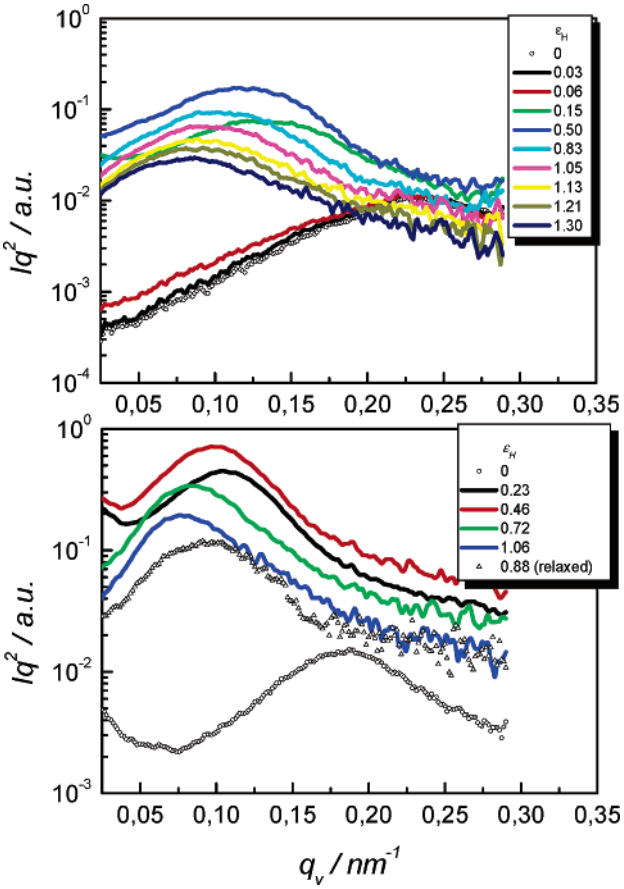

Figure 9. Plots of Iq^2 vs q_v at different deformations for PB18 (top) and PB57 (bottom). Peak positions were used to derive the thickness of the platelike cavitations.

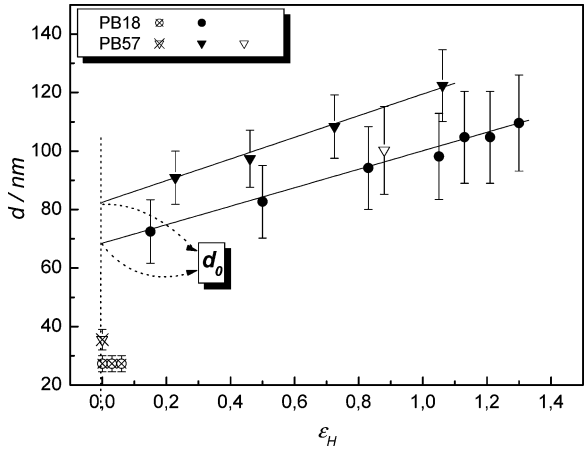

Figure 10. Long period (hollow plus cross symbol) and the thickness of the cavities along the stretching direction under stress (solid symbol) and relaxed (hollow symbol) as a function of strain. d_0 denotes the linear extrapolated thickness of the cavities at zero strain.

feature of the cavity formation. As was shown in Figure 6, cavities occur perpendicularly to the stress direction in those lamellar clusters whose normal is perpendicular to the stretching direction. The surroundings of those lamellar clusters undergo dominantly shear deformation and thus keep the optical refraction index essentially unchanged whereas the refraction index of those lamellar clusters with cavities included must change greatly. It is evident that these lamellar clusters possess a dimension of several hundred nanometers. It is thus believed that the heterogeneous distribution of the

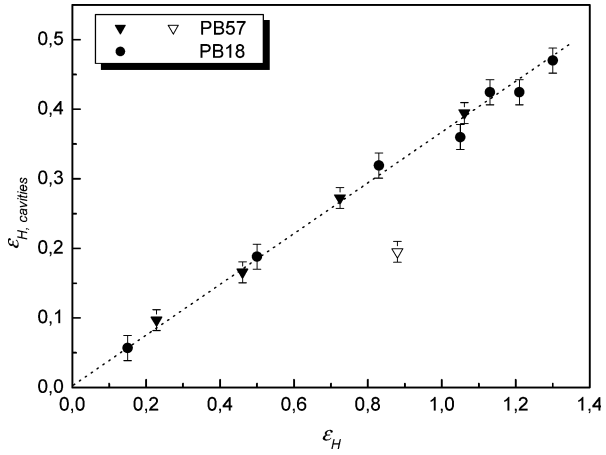

Figure 11. Strain of the cavities along the drawing direction ($\epsilon_{H,cavities} = \ln(d/d_0)$) of the two P1B samples as a function of the macroscopic strain (ϵ_H). The hollow symbol indicates the relaxed state.

cavities in the sample is the cause of the strong strain-whitening phenomenon.

Conclusions

In conclusion, USAXS provides an effective means to detect structure evolution on the nanometer length scale during tensile deformation of semicrystalline polymers. We have focused on the formation and evolution of cavities in P1B during tensile stretching. Cavities are responsible for the strain-whitening phenomenon in P1B. Scattering power analysis revealed that the volume fraction of the cavities is proportional to the crystallinity, indicating that the formation of the cavities is linked to the crystalline phase. It was found that at small deformations the cavities occur only in those lamellae whose normal are perpendicular to the stretching direction. This effect is due to the defective internal structure of the crystalline phase I lamellae of P1B. The main feature of the cavities is their platelike appearance with their normal parallel to the stretching direction at small deformation. At large deformations most cavities are oriented with their normal perpendicular to the stretching direction because of the preferential orientation of the polymer chains. The remaining cavities with their normal parallel to the stretching direction open in width with increasing macroscopic straining. Although the volume fraction of the cavities increases with the crystallinity, the strain of the cavities with their normal perpendicular to the stretching direction exhibits the same dependence on the macroscopic strain for the two P1B samples investigated.

Acknowledgment. We thank Dr. R. Gehrke and Ms. S. Cunis for assistance during USAXS experiments and data evaluation and Drs. H.-F. Enderle and D. Lilge for providing the sample of HDPE. We thank one of the referees for suggesting the consideration of the possible reflection of X-rays in our system and Prof. J. M. Schultz for providing citations on the problem.

References and Notes

(1) Gedde, U. W.; Wiebke, J.; Leijstrom, H.; Ifwarson, M. *Polym. Eng. Sci.* **1994**, *34*, 1773.
(2) Natta, G.; Corradini, P.; Bassi, I. W. *Nuovo Cimento Suppl.* **1960**, *15*, 52.
(3) Natta, G.; Pino, P.; Corradini, P.; Danusso, F.; Mantica, E.; Mazzanti, G. *J. Am. Chem. Soc.* **1955**, *77*, 1708.

(4) Boor, J.; Mitchell, J. C. *J. Polym. Sci.* **1963**, *A1*, 59.
(5) Hsu, T. C.; Geil, P. H. *J. Macromol. Sci., Phys.* **1985**, *B28*, 69.
(6) Yang, Y. C.; Geil, P. H. *Makromol. Chem.* **1985**, *186*, 1961.
(7) Weynant, E.; Haudin, J. M.; G'Sell, C. *J. Mater. Sci.* **1980**, *15*, 2677.
(8) Yee, R. Y.; Stein, R. S. *J. Polym. Sci.* **1970**, *A2*, 1661.
(9) Al-Hussein, M.; Strobl, G. *Macromolecules* **2002**, *35*, 8515.
(10) Sasaguri, K.; Hoshino, S.; Stein, R. S. *J. Appl. Phys.* **1964**, *35*, 47.
(11) Sasaguri, K.; Rhodes, M. B.; Stein, R. S. *J. Polym. Sci., Polym. Lett.* **1963**, *1*, 571.
(12) Yang, R. N.; Stein, R. S. *J. Polym. Sci.* **1967**, *A2*, 939.
(13) Karl, A.; Cunis, S.; Gehrke, R.; Krosigk, G. V.; Lode, U.; Luzinov, I.; Minko, S.; Pomper, T.; Senkovsky, V.; Voronov, A.; Wilke, W. *J. Macromol. Sci., Phys.* **1999**, *B38*, 901.
(14) Pedersen, J. S. In *Neutrons, X-rays and Light: Scattering Methods Applied to Soft Condensed Matter*; Lindner, P., Zemb, Th., Eds.; North-Holland: Amsterdam, 2002; p 127.
(15) Porod, G. In *Small-Angle X-ray Scattering*; Glatter, O., Kratky, O., Eds.; Academic Press: New York, 1982; p 35.
(16) Men, Y.; Strobl, G. *Chin. J. Polym. Sci.* **2002**, *20*, 161.
(17) Men, Y.; Strobl, G. *J. Macromol. Sci., Phys.* **2001**, *B40*, 775.
(18) Men, Y. F.; Rieger, J.; Strobl, G. *Phys. Rev. Lett.* **2003**, *91*, 095502.
(19) Peterlin, A. *J. Mater. Sci.* **1971**, *6*, 490.
(20) Hiss, R.; Hobeika, S.; Lynn, S.; Strobl, G. *Macromolecules* **1999**, *32*, 4390.
(21) Hobeika, S.; Men, Y.; Strobl, G. *Macromolecules* **2000**, *33*, 1827.
(22) Gohil, R. M.; Miles, M. J.; Petermann, J. *J. Macromol. Sci., Phys.* **1982**, *B21*, 189.
(23) Men, Y.; Strobl, G. *Polymer* **2002**, *43*, 2761.
(24) Strobl, G. *Eur. Phys. J. E* **2000**, *3*, 165.
(25) Schultz, J. M. *Acta Crystallogr.* **1971**, *A27*, 179.
(26) Tang, M. Y.; Fellers, J. F.; Lin, J. S. *J. Polym. Sci., Polym. Phys. Ed.* **1984**, *22*, 2215.
(27) Westbrook, P. A.; Fellers, J. F.; Cakmak, M.; Lin, J. S.; Hendricks, R. W. *J. Polym. Sci., Polym. Phys. Ed.* **1983**, *21*, 1913.
(28) Brown, H. R.; Kramer, E. J. *J. Macromol. Sci., Phys.* **1981**, *B19*, 487.
(29) Guinier, A.; Fournet, G. *Small Angle Scattering of X-rays*; John Wiley & Sons: New York, 1955.
(30) Shaw, J. P.; Gilbert, M. *J. Macromol. Sci., Phys.* **1991**, *B30*, 301.
(31) Castagnet, S.; Girault, S.; Gacougnolle, J. L.; Dang, P. *Polymer* **2000**, *41*, 7523.
(32) Athas database. http://web. utk. edu/~athas/, 2004.

MA048274K